Bracegirdle Thomas, J. (Orcid ID: 0000-0002-8868-4739)
Holmes Caroline, R. (Orcid ID: 0000-0002-3134-555X)
Hosking J. Scott (Orcid ID: 0000-0002-3646-3504)
Marshall Gareth (Orcid ID: 0000-0001-8887-7314)
Patterson Matthew, Ross (Orcid ID: 0000-0002-9484-8410)
Rackow Thomas (Orcid ID: 0000-0002-5468-575X)

Improvements in Circumpolar Southern Hemisphere Extratropical Atmospheric Circulation in CMIP6 Compared to CMIP

T. J. Bracegirdle[1]*, C. R. Holmes[1], J. S. Hosking[1], G. J. Marshall[1], M. Osman[2], M. Patterson[3], T. Rackow[4]

[1]British Antarctic Survey, Cambridge, UK.

[2] Centro de Investigaciones del Mar y la Atmósfera (CIMA/CONICET-UBA), Buenos Aires, Argentina.

[3]Atmospheric, Oceanic and Planetary Physics, University of Oxford, Oxford, UK

[4]Alfred Wegener Institute, Helmholtz Centre for Polar and Marine Research, Bremerhaven, Germany.

*Corresponding author: Thomas Bracegirdle (tjbra@bas.ac.uk)

Key Points:

- Improved representation of Southern Hemisphere mid-latitude tropospheric westerly jet in the Coupled Model Intercomparison Project Phase 6

- Key improvements are a reduced equatorward bias in jet latitude and more realistic timescales of variability

- There is no clear improvement in representation of the Amundsen Sea Low

Abstract

One of the major globally relevant systematic biases in previous generations of climate models has been an equatorward bias in the latitude of the Southern Hemisphere (SH) mid-latitude tropospheric eddy driven westerly jet. The far reaching implications of this for Southern Ocean heat and carbon uptake and Antarctic land and sea ice are key reasons why addressing this bias is a high priority. It is therefore of primary importance to evaluate the representation of the SH westerly jet in the latest generation of global climate and earth-system models that comprise the Coupled Model Intercomparison Project Phase 6 (CMIP6). In this paper we assess the representation of major indices of SH extratropical atmospheric circulation in CMIP6 by comparison against both observations and the previous generation of CMIP5 models. Indices assessed are the latitude and speed of the westerly jet, variability of the Southern Annular Mode (SAM) and representation of the Amundsen Sea Low (ASL). These are calculated from the historical forcing simulations of both CMIP5 and CMIP6 for time periods matching available observational and reanalysis datasets. From the 39 CMIP6 models available at the time of writing there is an overall reduction in the equatorward bias of the annual mean westerly jet from 1.9° in CMIP5 to 0.4° in CMIP6 and from a seasonal perspective the reduction is clearest in austral spring and summer. This is accompanied by a halving of the bias of SAM decorrelation timescales compared to CMIP5. However, no such overall improvements are evident for the ASL.

Plain Language Summary

Computer models that simulate the position, strength, and spatio-temporal behavior of winds in the Southern Hemisphere around the continent of Antarctica often show typical errors when compared to reality. This can impact answers to very relevant questions, such as how much heat and carbon are taken up by the ocean or how the sea ice cover will evolve in the future. Here we document how the newly available next generation of global climate models that form the basis for the next Assessment Report of the Intergovernmental Panel on Climate Change (IPCC) performs with respect to observed Southern Hemisphere winds. We also analyze potential improvements compared to the previous generation of computer models. Overall, some important differences to observations (biases) are much smaller than in the previous models (by up to 50%). Other diagnostics are, however, virtually unchanged, which indicates that the improvements are rather limited between model generations. However, our study could help to identify possible reasons for the remaining biases and to further reduce errors in upcoming models.

Keywords

CMIP6, CMIP5, Antarctic, Southern Ocean, westerly jet, Amundsen Sea Low.

1 Introduction

The circumpolar lower-tropospheric westerly winds over the Southern Ocean play a major role in the climate system both regionally and globally (Frölicher et al., 2015). In recent decades hemispheric-scale changes in these winds have been observed, characterized by changes in both speed and latitude of the zonal mean maximum (hereinafter referred to as the 'westerly jet') (). The most significant observed change has been a combined poleward shift and strengthening of the westerly jet caused primarily by stratospheric ozone depletion (Swart et al., 2015). This has been implicated in driving changes in Southern Ocean circulation, sea ice and Antarctic Peninsula temperatures (Marshall et al., 2006; Thompson et al., 2011).

Specific far-reaching consequences of changing westerlies that have been identified from model and observational studies are: (i) the westerly jet latitude impacts carbon storage in the deep Southern Ocean (Russell et al., 2006; Toggweiler et al., 2006); (ii) changing winds can affect the mass balance of Antarctica (Pritchard et al., 2012) and thus global sea level change; (iii) although poleward-shifting westerlies led to no discernible poleward migration of the Antarctic Circumpolar Current (Freeman et al., 2016; Gille, 2014), the strength of the Antarctic Polar Front has increased (Freeman et al., 2016) with possibly more efficient poleward eddy heat flux towards Antarctica (Hogg et al., 2008); (v) recent work also suggests that the strength of the westerlies controls Agulhas leakage of warm and salty ocean waters from the Indian Ocean to the South Atlantic Ocean (Durgadoo et al., 2013), with meridional shifts contributing to a lesser degree than previously asserted (Biastoch et al., 2009). Overall therefore, model biases in historical climatology and projected change of the westerly jet are a major concern for many aspects of the regional and global climate system.

Projections of 21st century climate change suggest further changes in the westerly jet associated both with expected stratospheric ozone recovery and increasing greenhouse gas concentrations (Barnes et al., 2014; Thompson et al., 2011). However, in previous generations of climate models the reliability of projections is affected by a prominent systematic equatorward bias in the mean-state westerly jet (Kidston & Gerber, 2010). Reducing this bias has been identified as one of the key priorities in developing the current generation of climate models (Stouffer et al., 2017). Data from the World Climate Research Programme's latest major international Coupled Model Intercomparison Project (CMIP) Phase 6 (Eyring et al., 2016) are now available and a key priority is therefore to compare the representation of mid-to-high latitude atmospheric circulation in CMIP6 against the previous generation of models that comprise CMIP5 (Taylor et al., 2012).

In this study, evaluation of the CMIP6 models is based on major indices of atmospheric variability over Southern Hemisphere (SH) mid-high latitudes: the Southern Annular Mode (SAM), the tropospheric westerly jet and the Amundsen Sea Low (ASL). The SAM is the leading pattern of atmospheric circulation variability in the SH. Its spatial characteristics and temporal evolution are usually described by the leading pattern from an empirical orthogonal function (EOF) analysis of geopotential height anomalies (Thompson & Wallace, 2000). The main spatial characteristic is the occurrence of geopotential height anomalies of opposite sign at SH mid-latitudes and over Antarctica. This aspect is captured in SAM indices based on differences between zonal means in geopotential height or mean sea-level pressure at mid (40°S) and high (65°S) latitudes (Gong & Wang, 1999). A key advantage of the zonal mean diagnostic is that it can be reconstructed from in-situ sea-level pressure observations from a widespread network introduced during the International Geophysical Year in 1958 (Marshall, 2003).

Positive indices of the SAM by convention represent periods of below-average pressure or geopotential height over Antarctica and above-average values at mid-latitudes. In terms of atmospheric dynamics, positive (negative) SAM indices are linked to stronger (weaker) and/or more poleward (equatorward) phases of the westerly jet (e.g. (Swart et al., 2015)). Strengthening/weakening of the westerly jet does not necessarily occur along with poleward/equatorward shifting and therefore jet diagnostics can provide an additional level of understanding in terms of variability, trends, drivers and impacts of the SAM (Baker et al., 2017; McGraw & Barnes, 2016).

The EOF spatial patterns are best described by this zonal-mean variation during austral summer (DJF), but also include a distinct non-annular component in winter (JJA) (Fogt et al., 2012a). The main non-annular feature of atmospheric circulation around Antarctica is the ASL (Turner et al., 2013). The ASL is a climatological minimum in sea-level pressure that exhibits a seasonal migration between the Ross Sea (~150°W) in June and the Bellingshausen Sea (~110°W) in January. Variability in ASL longitude has a major influence on regional sea ice, precipitation and temperature over and adjacent to West Antarctica (Hosking et al., 2013; Raphael et al., 2016). A good representation of the climatological ASL is therefore highly important to the climate of West Antarctica, a region of global relevance due to highly sensitive and rapidly changing land and sea ice e.g. (Holland et al., 2019).

Previous generations of climate models have exhibited a range of success in terms of representing the above atmospheric indices. The equatorward bias in the westerly jet was identified in the CMIP3 models by (Kidston & Gerber, 2010), with values on average of approximately 4° in latitude. In CMIP5 this was reduced a little overall, but still with an annual mean bias of 3.3° (Bracegirdle et al., 2013). The equatorward westerly jet bias is not clearly evident in time mean SAM indices, since these are generally normalized to a recent baseline period, such as 1970-1999. However, a systematic bias in too long persistence of the SAM has been identified in CMIP3 and CMIP5, with decorrelation timescales of typically ~20 days compared to reanalysis estimates of ~10 days. Kidston and Gerber (2010) found that these biases are correlated with jet latitude bias across different models (longer timescales correspond to models with a larger equatorward bias). The CMIP5 models do not exhibit a clear positive or negative bias in jet speed (i.e. clearly within the spread of different models) (Bracegirdle et al., 2013).

With regard to non-annular circulation patterns, climate models to date show a mixed picture in terms of success in representing the ASL (Hosking et al., 2016). Most CMIP5 models have clear biases that are most evident in longitudinal position, which therefore affects the realism in the associated simulated climate of West Antarctica. Hosking et al. (2016) suggested that a subset of 11 (from 49) CMIP5 models can be considered to satisfactorily represent the annual cycle of the ASL.

The aim of this study is to determine whether the representation of the SAM, westerly jet and/or ASL has improved in the newly available earth system and climate model simulations that have been coordinated as part of CMIP6. Output from CMIP6 historical forcing simulations is compared against both observational/reanalysis data and output from the CMIP5 archive. The data sources and analysis methods are described in Section 2 followed by results in Section 3 and conclusions in Section 4.

2 Materials and Methods

2.1 Climate model and reanalysis data

Climate model data from both CMIP5 and CMIP6 were used. The variables analyzed were monthly mean zonal wind on pressure levels (variable name 'ua'), daily and monthly mean atmospheric pressure at mean sea level (variable name 'psl') and daily mean geopotential height on pressure levels (variable name 'zg'). Output from the first available ensemble member of all available CMIP5 and CMIP6 'historical' simulations were used. Historical simulations are free-running fully coupled model runs that include known natural and anthropogenic external climate forcings from the mid-19th century to present day. The specific CMIP5 and CMIP6 models used in this study are detailed in Tables 1 and 2.

Observationally-constrained estimates of actual conditions were taken mainly from two reanalysis datasets: the European Centre for Medium-Range Weather Forecasts ERA-Interim (Dee et al., 2011) and NCEP-DOE Reanalysis 2 (NCEP) (Kanamitsu et al., 2002) re-analyses. For westerly jet and ASL diagnostics just ERA-Interim was used since it has been found to perform relatively well over Antarctica and the Amundsen Sea region (Bracegirdle, 2013; Bracegirdle & Marshall, 2012) and also exhibit very similar results to other re-analyses for westerly jet diagnostics (Bracegirdle et al., 2013; Swart & Fyfe, 2012) and ASL diagnostics (Fogt et al., 2012b) with inter-reanalysis differences an order of magnitude smaller than the range across CMIP models. For the decorrelation timescale analysis, the NCEP reanalysis was also used as a check for possible reanalysis sensitivity on shorter daily timescales.

2.2 Circulation diagnostics

2.2.1 Station-based SAM index

The station based SAM index was developed by Marshall (2003) and is referred to hereinafter as SAM$_{stn}$. It is based on mean sea level pressure data from 12 meteorological stations, 6 located at SH mid-latitudes (~40ºS) and a further 6 around the Antarctic coastline (~65ºS). The SAM$_{stn}$ index value is calculated as the normalized difference between the mean station pressure at 40ºS and 65ºS. To reconstruct the same index in gridded model output, model data were interpolated to the station locations to the nearest 0.1º lat./lon.

2.2.2 EOF-based SAM index and decorrelation timescales

The EOF-based SAM was computed following (Gerber et al., 2010) and is referred to hereinafter as SAM$_{EOF}$. The method involves calculating the SAM$_{EOF}$ using the first principal component time series of daily zonal mean geopotential height at 500 hPa, after the data have been deseasonalized, detrended and the global mean removed. As in Gerber et al. (2010), zonal means are used to reduce the amount of data required for the analysis. EOFs are calculated for the region south of 20°S and anomalies are weighted by the square root of the cosine of latitude to account for the reduction in area at the poles. The diagnostic used is the decorrelation timescale, which is the e-folding timescale of the autocorrelation function of the SAM index. It is calculated by taking a 180 day window around a given day, smoothing it with a Gaussian filter with a full width at half maximum of 60 days and then calculating lagged correlations. The decorrelation timescale for a given point in the seasonal cycle is the average decorrelation timescale on that day over the period of study. At the time of writing the daily field required for this analysis were only available for 17 of the CMIP6 models, which is noted in Table 1.

2.2.2 Tropospheric westerly jet

The tropospheric westerly jet was diagnosed from monthly-mean zonally-averaged 850 hPa zonal wind output from gridded reanalysis and CMIP model output. For each monthly-mean field, the maximum in the zonal mean between 75°S and 10°S defines the jet speed index (JSI) at the position of this maximum defines the jet latitude index (JLI). Seasonal and annual means were created after first computing jet diagnostics from the monthly fields.

2.2.3 Amundsen Sea Low

The Amundsen Sea Low index (ASL) follows Hosking et al. (2016). Up to six lows in the monthly mean sea level pressure field in SH mid to high latitudes were identified by a minima-finding algorithm. The ASL is the lowest such feature which falls within the ASL region defined as 60-80S, 170-298E. The ASL index constitutes the longitude, latitude and relative central pressure of this feature, where the relative pressure is the actual local pressure minus the ASL region average pressure. The ASL relative central pressure therefore captures local variability in the pressure field without aliasing the effects of zonal mean variability, thus capturing the effect on local climate (Hosking et al., 2013). The ASL was calculated on each model's native grid, for both CMIP5 and CMIP6. Here seasonal errors from ERA-interim are shown, calculated from the monthly index.

4 Results

The time evolution of CMIP6-simulated SH zonal-mean circulation patterns over the period since the mid 19th century shows the well-established increasingly positive polarity of the SAM since the late 1970s (Figure 1), which is most pronounced in summer (DJF) in association with stratospheric ozone depletion (Arblaster & Meehl, 2006; Marshall, 2003). Comparisons against observations and re-analyses in Figure 1 indicate that the CMIP6 models are broadly successful in reproducing the real-world strength of these summer SAM_{stn} trends and their link to combined poleward shifting and strengthening of the tropospheric westerly jet.
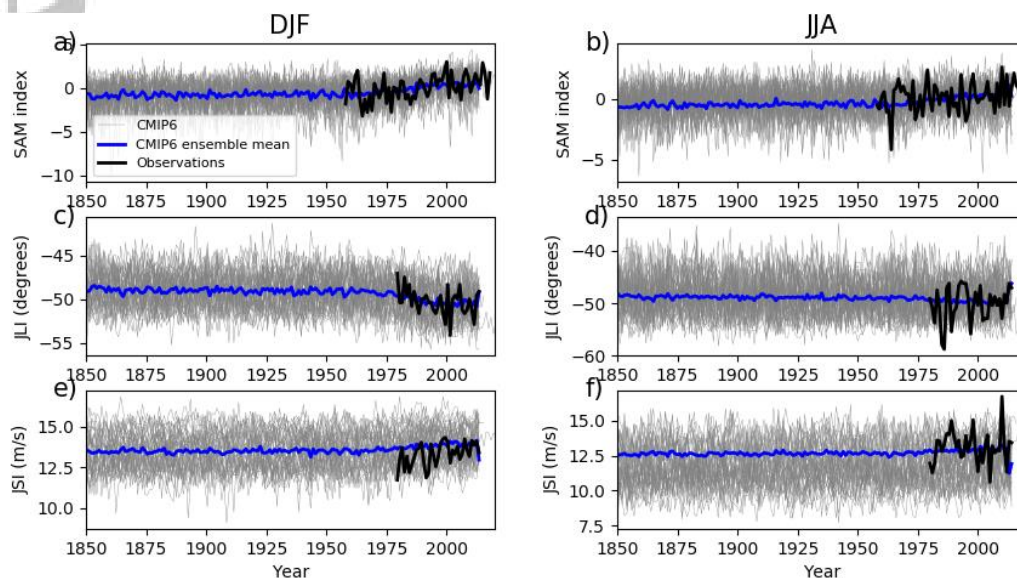

Figure 1. Time series of key SH circulation indices for summer (DJF) (a, c, e) and winter (JJA) (b, d, f). Each row from the top shows: Station-based SAM_{stn} index (a, b), Jet Latitude Index (JLI) (c, d), and Jet Speed Index (JSI) (e, f). CMIP6 model data are shown in blue, with reanalysis (ERA-Interim) or observations in the thick black solid lines.

From a climatological perspective, Figure 2a shows that, as for previous CMIP ensembles (Bracegirdle et al., 2013; Kidston & Gerber, 2010), the CMIP6 models exhibit an equatorward JLI bias, which is most prevalent in winter (JJA) (Figure 3). A key question highlighted in the Introduction is whether the equatorward jet bias is reduced in the CMIP6 ensemble compared to CMIP5. Figure 2a shows that this is the case for annual mean JLI, with a CMIP6 ensemble mean bias of 0.4° compared to 1.9° in CMIP5. Values for individual models are shown in Tables 3 and 4. Seasonally the largest reductions in bias are in spring (SON) and summer (DJF), with smaller improvements in autumn and winter (Figure 3).
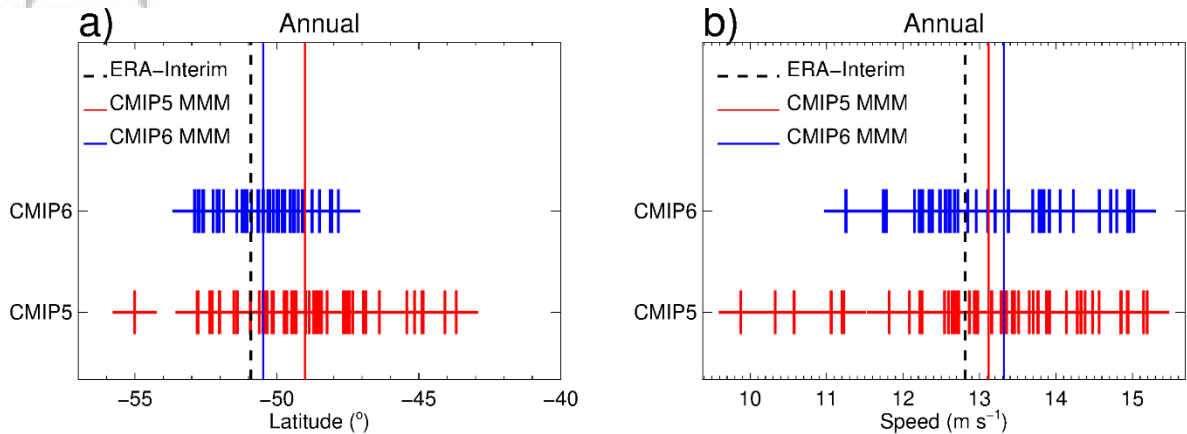
Figure 2. Southern Hemisphere JLI (a) and JSI (b) time slice climatologies over 1980-2005. Each cross represents an individual historical simulation from CMIP6 (blue) and CMIP5 (red) with the multi-model mean (MMM) for each shown by the vertical solid lines. Re-analysis estimates from ERA-Interim are shown by the black vertical dashed lines.

Alongside the reduction in ensemble mean equatorward JLI bias, there is a reduction in the inter-model spread in CMIP6 compared to CMIP5. For annual mean JLI the standard deviation of the inter-model spread is 1.4° in CMIP6 compared to 2.5° in CMIP5.
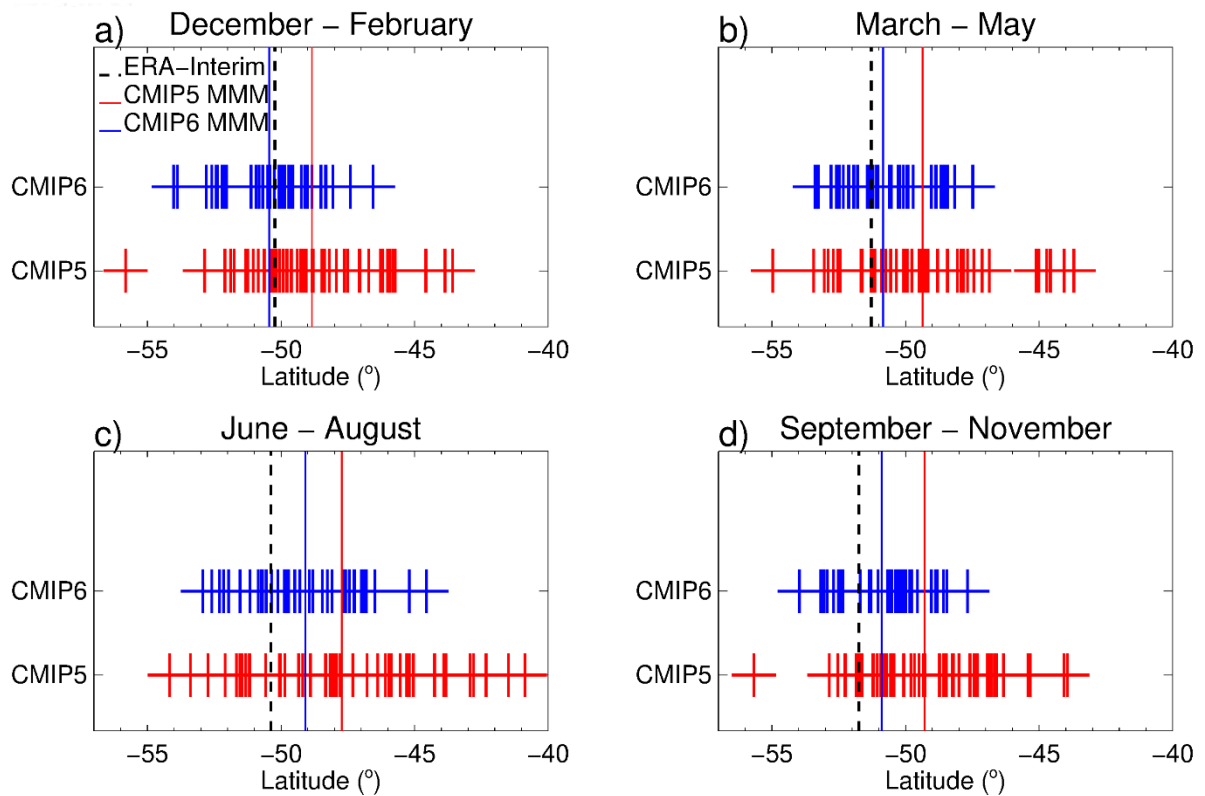
Figure 3. As Figure 2a, but for individual seasons.

Since at the time of writing an initial subset of 39 of the full CMIP6 dataset was available, it is possible that the reduction in equatorward bias in CMIP6 may not be robust to the addition of further CMIP6 models. To assess the likelihood of this, multi-model mean JLI values were calculated from 10,000 pseudo-randomly-generated CMIP5 sub-ensembles of size 39. The frequency distribution of these sub-ensemble means is shown in Figure 4. This shows that the CMIP6 ensemble mean JLI from the 39 available CMIP6 models sits outside the 95% confidence interval of the randomly-generated CMIP5 sub-ensembles. The implication is that the reduced equatorward jet stream bias is statistically significant and likely to be robust as further data are added to the CMIP6 archive. Further support for this conclusion is that all but two of the CMIP5 models with JLI values the upper quartile (i.e. the 12 most equatorward) of the CMIP5 range have either direct descendants or models from the same model centers in the CMIP6 ensemble (Table 5). Figure 4b further shows that the reduction in inter-model spread apparent between CMIP6 and CMIP5 also appears robust.
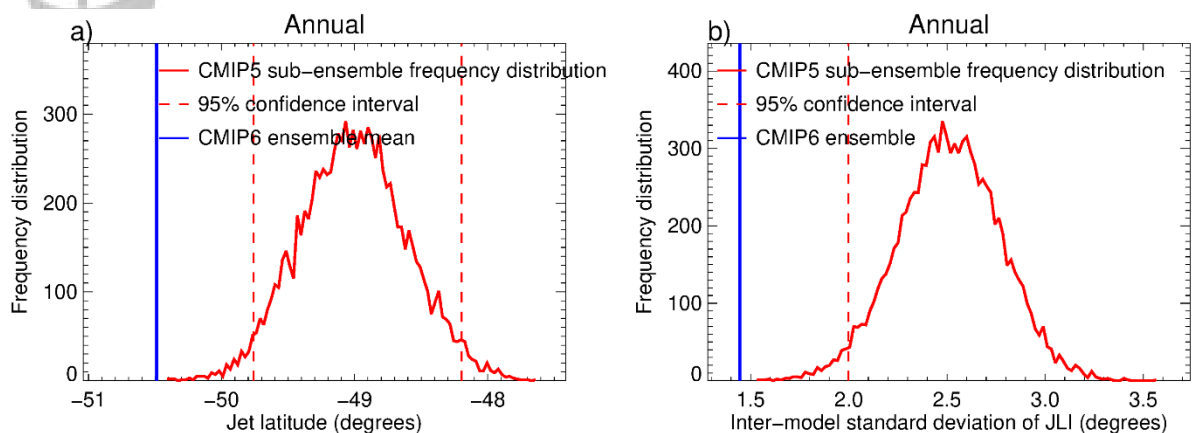
Figure 4. The red solid line shows the frequency distribution of ensemble mean (a) and ensemble standard deviation (b) of JLI calculated from 10,000 pseudo-randomly-generated CMIP5 sub-ensembles of size n=39 taken from the 47 available CMIP5 models (i.e. a bootstrapping method). The vertical dashed red lines show the 95% confidence interval (2.5th and 97.5th percentiles). The CMIP6 ensemble mean and standard deviation are shown by the vertical solid blue lines.

The above improvements in JLI representation are not matched by evidence for improvements in JSI in CMIP6 compared to CMIP5. Both CMIP6 and CMIP5 exhibit ensemble mean annual mean JSI values that are biased slightly too high compared to ERA-Interim (biases of 0.5 and 0.3 m s^{-1} respectively) (Figure 2b and Tables 3 and 4). Results for individual models are shown in Figure 4. There is no clear CMIP6-to-CMIP5 reduction in inter-model spread, with only a small (18%) reduction in inter-model standard deviation. It is notable that the biases in jet speed are both smaller than for jet latitude and also do not exhibit a clear reduction in spread between CMIP5 and CMIP6. Possible explanations for this will be provided in the Discussion section.
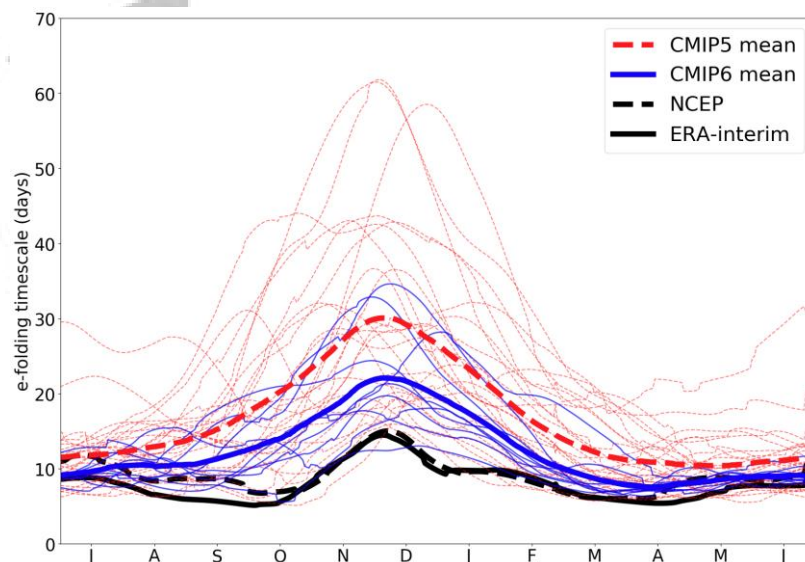

Figure 5. SAM$_{EOF}$ decorrelation time-scale as a function of season. CMIP5 models are shown in thin red dashed lines and CMIP6 models in solid blue lines. The multi-model means are thicker red dashed and solid blue lines for CMIP5 and CMIP6 respectively, while ERA-Interim (solid black) and NCEP reanalysis (dashed black) values are also shown for comparison.

To provide more insight into the above-described time-mean differences, SAM$_{EOF}$ decorrelation timescales were assessed. This gives a broader picture of whether the reductions in jet latitude bias in CMIP6 are accompanied by improved representation of atmospheric eddies and their feedbacks (Kidston & Gerber, 2010). Figure 5 shows the SAM$_{EOF}$ decorrelation time-scale as a function of season for CMIP5 and CMIP6. Overall CMIP6 models present a significant improvement in the representation of SAM timescale for most of the months but especially in mid November, where the biases is reduced from around 30 days for CMIP5 to near 20 days in CMIP6. Even with just 17 models, the same bootstrapping approach that was applied to JLI sub-ensembles indicates again statistical significance of the CMIP6 improvements (not shown). Despite large reductions, these timescales are still longer than the timescale obtained from ERA-Interim (around 15 days).

As might be expected from the previously documented link between jet latitude and decorrelation timescale, the months of largest improvement are coincident with the seasons of clearest improvement in JLI, which are austral spring and summer (Figure 3).

The improvements in the austral winter season are smaller and less statistically significant than for summer, at least in the zonally averaged diagnostics evaluated so far. This is notable since zonal asymmetries are at their most pronounced in winter at mid-high latitudes in the Southern Hemisphere.
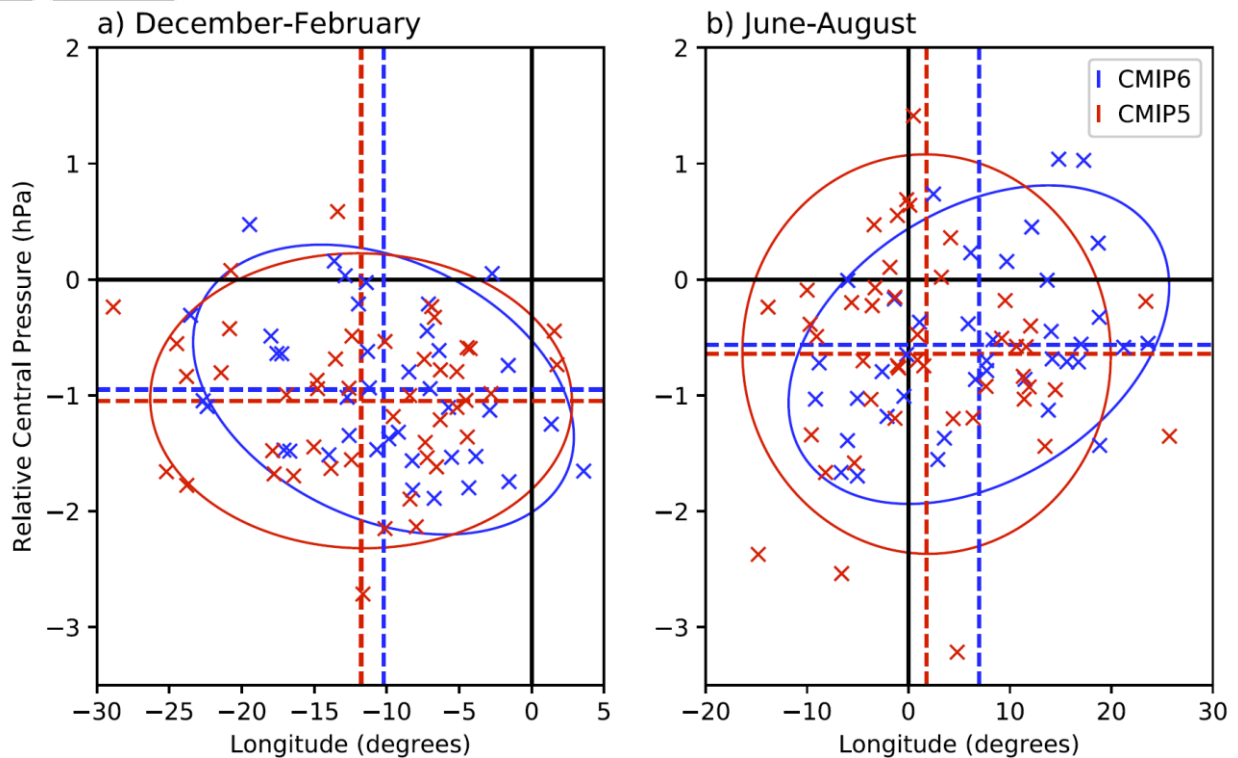
Figure 6. ASL summer (**a**) and winter (**b**) climatological longitude and relative central pressure biases from ERA-Interim for CMIP5 (red) and CMIP6 (blue) models. The solid black lines show zero bias. Dashed lines show the multi-model mean and the ellipses depict the two standard deviation confidence interval.

The main feature of the zonally asymmetric atmospheric circulation around Antarctica is the ASL. Here we show key measures of the ASL diagnosed from CMIP6, CMIP5 and reanalysis data in summer and winter (Figure 6). In terms of longitude, the ensemble mean of the CMIP6 models exhibits a climatological westward bias of ~10 degrees in summer (DJF, left panel of Figure 6), which is very similar to the CMIP5 ensemble mean bias of ~12 degrees. In winter both CMIP5 and CMIP6 exhibit an ensemble mean eastward bias (Figure 6, right panel), which is larger in CMIP6 (8 degrees) and only 2 degrees in CMIP5. However, there is a large overlap between the ranges spanned by the two ensembles and therefore no clear separation.

The clearest bias in Figure 6 is that the majority of CMIP6 and CMIP5 models exhibit too deep relative central pressures that are most apparent in austral summer (-1.0 hPa) but also apparent in winter (-0.5 hPa). For this diagnostic both model generations are very similar.

Multi-model mean ASL latitude bias is small in both generations (+0.4 degrees in CMIP5 and +0.3 degrees in CMIP6 for JJA, and +0.3deg in CMIP5 and -0.2deg in CMIP6 for DJF; not shown). However, for both seasons, the model spread in CMIP6 is reduced compared to CMIP5.

5 Conclusions

An evaluation of the representation of atmospheric circulation at extratropical latitudes in the newly available CMIP6 dataset is presented. The evaluations are based on comparison between major modes of variability calculated from CMIP6 model output and data from observations and reanalyses. The question of whether the CMIP6 ensemble improves on previous generations of models is also addressed by comparison against CMIP5 data.

Overall the CMIP6 models exhibit a reduced ensemble-mean equatorward bias of the mid-latitude SH eddy driven jet compared to CMIP5 (0.4° in CMIP6 compared to 1.9° in CMIP5). A caveat is that this is based on 21 models for which data were available at the time of writing and that more model data will potentially affect this conclusion. However, a random resampling of 10,000 CMIP5 sub-ensembles of size 39 provides statistical evidence of a significant improvement.

Improvements in jet position are accompanied by reduced biases in jet variability quantified by decorrelation timescales of the SAM. Improvements are evident for most months and clearest in November (~30 days for CMIP5 to near 21 days in CMIP6). Nevertheless, timescales remain longer than in ERA-Interim (~15 days for November). Although the necessary daily data were only available from 17 models, similar to jet latitude improvements a random resampling suggests a statistically significant improvement on CMIP5. Although this suggests improved representation of eddy feedbacks, causality is difficult to establish from the initial analysis presented. Other factors may also play a role by influencing the atmospheric basic state that control eddy growth and propagation. One clue to identifying reasons for reduced latitude bias in CMIP6, is that the CMIP5-CMIP6 differences are much smaller for JSI than for JLI. Some drivers of jet bias are more closely linked to latitude than speed e.g. (Baker et al., 2017). For example SH mid-latitude short-wave cloud bias over the Southern Ocean was found in the CMIP5 models to be strongly linked to jet latitude (Ceppi et al., 2012) and Southern Ocean sea-surface temperature (Hyder et al., 2018).

Despite improvements in representing the zonally-averaged circulation as diagnosed from westerly jet and SAM diagnostics, no clear improvements in representation of the ASL are evident between CMIP5 and CMIP6. On average both model generations exhibit too weak relative central pressures. One possible reason for the lack of improvement is that the grid spacing of standard-configuration CMIP6 models is broadly very similar to CMIP5 (not shown), which suggests that the representation of Antarctic orography, and its known influence on Antarctic circulation zonal asymmetries such as the ASL (Lachlan-Cope et al., 2001; van Niekerk et al., 2017), may not have improved. Due to strong ocean-atmosphere-ice coupling in the region, these ASL biases are a potentially important driver of regional surface climate biases in many of the CMIP6 models (Hosking et al., 2013).

However, there are indications that improvements in circumpolar circulation may have contributed to the generally improved simulation of the mean state of Antarctic sea ice in

CMIP6 models relative to CMIP5 (Roach et al., 2020) and the study of further possible positive links to other oceanic quantities, such as the representation of ocean heat transport near Antarctica, will be a topic for future studies.

References

Arblaster, J. M., & Meehl, G. A. (2006). Contributions of external forcings to southern annular mode trends. *Journal of Climate, 19*(12), 2896-2905. doi:10.1175/JCLI3774.1

Baker, H. S., Woollings, T., & Mbengue, C. (2017). Eddy-Driven Jet Sensitivity to Diabatic Heating in an Idealized GCM. *Journal of Climate, 30*(16), 6413-6431. doi:10.1175/jcli-d-16-0864.1

Barnes, E. A., Barnes, N. W., & Polvani, L. M. (2014). Delayed Southern Hemisphere Climate Change Induced by Stratospheric Ozone Recovery, as Projected by the CMIP5 Models. *Journal of Climate, 27*(2), 852-867. doi:10.1175/jcli-d-13-00246.1

Biastoch, A., Boning, C. W., Schwarzkopf, F. U., & Lutjeharms, J. R. E. (2009). Increase in Agulhas leakage due to poleward shift of Southern Hemisphere westerlies. *Nature, 462*(7272), 495-U188. doi:10.1038/nature08519

Bracegirdle, T. J. (2013). Climatology and recent increase of westerly winds over the Amundsen Sea derived from six reanalyses. *International Journal of Climatology, 33*(4), 843-851. doi:10.1002/joc.3473

Bracegirdle, T. J., & Marshall, G. J. (2012). The reliability of Antarctic tropospheric pressure and temperature in the latest global reanalyses. *Journal of Climate, 25*(20), 7138-7146. doi:10.1175/JCLI-D-11-00685.1

Bracegirdle, T. J., Shuckburgh, E., Sallee, J.-B., Wang, Z., Meijers, A. J. S., Bruneau, N., et al. (2013). Assessment of surface winds over the Atlantic, Indian, and Pacific Ocean sectors of the Southern Ocean in CMIP5 models: historical bias, forcing response, and state dependence. *Journal of Geophysical Research - Atmospheres, 118*(2), 547-562. doi:10.1002/jgrd.50153

Ceppi, P., Hwang, Y. T., Frierson, D. M. W., & Hartmann, D. L. (2012). Southern Hemisphere jet latitude biases in CMIP5 models linked to shortwave cloud forcing. *Geophysical Research Letters, 39*. doi:10.1029/2012gl053115

Dee, D. P., Uppala, S. M., Simmons, A. J., Berrisford, P., Poli, P., Kobayashi, S., et al. (2011). The ERA-Interim reanalysis: configuration and performance of the data assimilation system. *Quarterly Journal of the Royal Meteorological Society, 137*(656), 553-597. doi:10.1002/qj.828

Durgadoo, J. V., Loveday, B. R., Reason, C. J. C., Penven, P., & Biastoch, A. (2013). Agulhas Leakage Predominantly Responds to the Southern Hemisphere Westerlies. *Journal of Physical Oceanography, 43*(10), 2113-2131. doi:10.1175/jpo-d-13-047.1

Eyring, V., Bony, S., Meehl, G. A., Senior, C. A., Stevens, B., Stouffer, R. J., & Taylor, K. E. (2016). Overview of the Coupled Model Intercomparison Project Phase 6 (CMIP6) experimental design and organization. *Geoscientific Model Development, 9*(5), 1937-1958. doi:10.5194/gmd-9-1937-2016

Fogt, R. L., Jones, J. M., & Renwick, J. (2012a). Seasonal Zonal Asymmetries in the Southern Annular Mode and Their Impact on Regional Temperature Anomalies. *Journal of Climate, 25*(18), 6253-6270. doi:10.1175/jcli-d-11-00474.1

Fogt, R. L., Wovrosh, A. J., Langen, R. A., & Simmonds, I. (2012b). The characteristic variability and connection to the underlying synoptic activity of the Amundsen-Bellingshausen Seas Low. *Journal of Geophysical Research-Atmospheres, 117*. doi:D07111
10.1029/2011jd017337

Freeman, N. M., Lovenduski, N. S., & Gent, P. R. (2016). Temporal variability in the Antarctic Polar Front (2002-2014). *Journal of Geophysical Research-Oceans, 121*(10), 7263-7276. doi:10.1002/2016jc012145

Frölicher, T. L., Sarmiento, J. L., Paynter, D. J., Dunne, J. P., Krasting, J. P., & Winton, M. (2015). Dominance of the Southern Ocean in Anthropogenic Carbon and Heat Uptake in CMIP5 Models. *Journal of Climate, 28*(2), 862-886. doi:10.1175/jcli-d-14-00117.1

Gerber, E. P., Baldwin, M. P., Akiyoshi, H., Austin, J., Bekki, S., Braesicke, P., et al. (2010). Stratosphere-troposphere coupling and annular mode variability in chemistry-climate models. *Journal of Geophysical Research-Atmospheres, 115*. doi:10.1029/2009jd013770

Gille, S. T. (2014). Meridional displacement of the Antarctic Circumpolar Current. *Philosophical Transactions of the Royal Society a-Mathematical Physical and Engineering Sciences, 372*(2019). doi:10.1098/rsta.2013.0273

Gong, D., & Wang, S. (1999). Definition of Antarctic oscillation index. *Geophysical Research Letters, 26*(4), 459-462. doi:10.1029/1999GL900003. (Accession No. 3980)

Hogg, A. M., Meredith, M. P., Blundell, J. R., & Wilson, C. (2008). Eddy heat flux in the Southern Ocean: Response to variable wind forcing. *Journal of Climate, 21*(4), 608-620. doi:10.1175/2007jcli1925.1

Holland, P. R., Bracegirdle, T. J., Dutrieux, P., Jenkins, A., & Steig, E. J. (2019). West Antarctic ice loss influenced by internal climate variability and anthropogenic forcing. *Nature Geoscience, 12*(9), 718-724. doi:10.1038/s41561-019-0420-9

Hosking, J. S., Orr, A., Bracegirdle, T. J., & Turner, J. (2016). Future circulation changes off West Antarctica: Sensitivity of the Amundsen Sea Low to projected anthropogenic forcing. *Geophysical Research Letters, 43*(1), 367-376. doi:10.1002/2015gl067143

Hosking, J. S., Orr, A., Marshall, G. J., Turner, J., & Phillips, T. (2013). The influence of the Amundsen-Bellingshausen Seas Low on the climate of West Antarctica and its representation in coupled climate model simulations. *Journal of Climate*, in press. doi:10.1175/JCLI-D-12-00813.1

Hyder, P., Edwards, J. M., Allan, R. P., Hewitt, H. T., Bracegirdle, T. J., Gregory, J. M., et al. (2018). Critical Southern Ocean climate model biases traced to atmospheric model cloud errors. *Nature Communications, 9*. doi:10.1038/s41467-018-05634-2

Kanamitsu, M., Ebisuzaki, W., Woollen, J., Yang, S. K., Hnilo, J. J., Fiorino, M., & Potter, G. L. (2002). NCEP-DOE AMIP-II reanalysis (R-2). *Bulletin of the American Meteorological Society, 83*(11), 1631-1643. doi:10.1175/bams-83-11-1631(2002)083<1631:nar>2.3.co;2

Kidston, J., & Gerber, E. P. (2010). Intermodel variability of the poleward shift of the austral jet stream in the CMIP3 integrations linked to biases in 20th century climatology. *Geophysical Research Letters, 37*, L09708. doi:10.1029/2010gl042873

Lachlan-Cope, T. A., Connolley, W. M., & Turner, J. (2001). The role of the non-axisymmetric Antarctic orography in forcing the observed pattern of variability of the Antarctic climate. *Geophysics Research Letters, 28*, 4111-4114.

Marshall, G. J. (2003). Trends in the Southern Annular Mode from observations and reanalyses. *Journal of Climate, 16*, 4134-4143. doi:10.1175/1520-0442(2003)016<4134:TITSAM>2.0.CO;2

Marshall, G. J., Orr, A., van Lipzig, N. P. M., & King, J. C. (2006). The impact of a changing Southern Hemisphere Annular Mode on Antarctic Peninsula summer temperatures. *Journal of Climate, 19*(20), 5388-5404. Retrieved from <Go to ISI>://000241755900020

McGraw, M. C., & Barnes, E. A. (2016). Seasonal Sensitivity of the Eddy-Driven Jet to Tropospheric Heating in an Idealized AGCM. *Journal of Climate, 29*(14), 5223-5240. doi:10.1175/jcli-d-15-0723.1

Pritchard, H. D., Ligtenberg, S. R. M., Fricker, H. A., Vaughan, D. G., van den Broeke, M. R., & Padman, L. (2012). Antarctic ice-sheet loss driven by basal melting of ice shelves. *Nature, 484*(7395), 502-505. doi:10.1038/nature10968

Raphael, M. N., Marshall, G. J., Turner, J., Fogt, R. L., Schneider, D., Dixon, D. A., et al. (2016). The Amundsen Sea Low: Variability, Change, and Impact on Antarctic Climate. *Bulletin of the American Meteorological Society, 97*(1), 111-121. doi:10.1175/bams-d-14-00018.1

Roach, L. A., Dorr, J., Holmes, C. R., Massonnet, F., Blockley, E. W., Rackow, T., et al. (2020). Antarctic Sea Ice in CMIP6. *Geophysical Research Letters, in press*. doi:10.1029/2019GL086729

Russell, J. L., Dixon, K. W., Gnanadesikan, A., Stouffer, R. J., & Toggweiler, J. R. (2006). The Southern Hemisphere westerlies in a warming world: Propping open the door to the deep ocean. *Journal of Climate, 19*(24), 6382-6390. doi:10.1175/jcli3984.1

Stouffer, R. J., Eyring, V., Meehl, G. A., Bony, S., Senior, C., Stevens, B., & Taylor, K. E. (2017). CMIP5 scientific gaps and recommendations for CMIP6. *Bulletin of the American Meteorological Society, 98*(1), 95-105. doi:10.1175/bams-d-15-00013.1

Swart, N. C., & Fyfe, J. C. (2012). Observed and simulated changes in the Southern Hemisphere surface westerly wind-stress. *Geophysical Research Letters, 39*(16), L16711. doi:10.1029/2012gl052810

Swart, N. C., Fyfe, J. C., Gillett, N., & Marshall, G. J. (2015). Comparing Trends in the Southern Annular Mode and Surface Westerly Jet. *Journal of Climate, 28*(22), 8840-8859. doi:10.1175/jcli-d-15-0334.1

Taylor, K. E., Stouffer, R. J., & Meehl, G. A. (2012). An Overview of CMIP5 and the Experiment Design. *Bulletin of the American Meteorological Society, 93*, 485–498. doi:10.1175/bams-d-11-00094.1

Thompson, D. W. J., Solomon, S., Kushner, P. J., England, M. H., Grise, K. M., & Karoly, D. J. (2011). Signatures of the Antarctic ozone hole in Southern Hemisphere surface climate change. *Nature Geoscience, 4*(11), 741-749. doi:10.1038/ngeo1296

Thompson, D. W. J., & Wallace, J. M. (2000). Annular modes in the extratropical circulation. Part I: month-to-month variability. *Journal of Climate, 13*, 1000-1016.

Toggweiler, J. R., Russell, J. L., & Carson, S. R. (2006). Midlatitude westerlies, atmospheric CO2, and climate change during the ice ages. *Paleoceanography, 21*(2). doi:10.1029/2005pa001154

Turner, J., Phillips, T., Hosking, J. S., Marshall, G. J., & Orr, A. (2013). The Amundsen Sea low. *International Journal of Climatology, 33*(7), 1818-1829. doi:10.1002/joc.3558

van Niekerk, A., Scinocca, J. F., & Shepherd, T. G. (2017). The Modulation of Stationary Waves, and Their Response to Climate Change, by Parameterized Orographic Drag. *Journal of the Atmospheric Sciences, 74*(8), 2557-2574. doi:10.1175/jas-d-17-0085.1

Table 1

CMIP5 models and variables used

Number	Model name	Model center	ua	psl	zg*
1	ACCESS1.0	CSIRO-BOM	x	x	x
2	ACCESS1.3	CSIRO-BOM	x	x	x
3	BCC-CSM1.1	BCC	x	x	x
4	BCC-CSM1.1(m)	BCC	x	x	x
5	BNU-ESM	GCESS	x	x	x
6	CCSM4	NCAR	x	x	
7	CESM1-BGC	NSF-DOE-NCAR	x	x	
8	CESM1(CAM5)	NSF-DOE-NCAR	x	x	
9	CESM1-FASTCHEM	NSF-DOE-NCAR	x	x	
10	CESM1(WACCM)	NSF-DOE-NCAR	x	x	
11	CMCC-CESM	CMCC	x	x	x
12	CMCC-CM	CMCC	x	x	x
13	CMCC-CMS	CMCC	x	x	x
14	CNRM-CM5	CNRM-CERFACS	x	x	x
15	CNRM-CM5-2	CNRM-CERFACS	x	x	
16	CSIRO-MK3.6.0	CSIRO-QCCCE	x	x	
17	CanCM4	CCCma	x	x	
18	CanESM2	CCCma	x	x	
19	EC-EARTH	EC-EARTH			x
20	FGOALS-g2	LASG-CESS	x	x	x
21	FIO-ESM	FIO	x	x	
22	GFDL-CM2p1	NOAA GFDL	x	x	
23	GFDL-CM3	NOAA GFDL	x	x	
24	GFDL-ESM2G	NOAA GFDL	x	x	
25	GFDL-ESM2M	NOAA GFDL	x	x	

			ua	psl	zg
26	GISS-E2-H	NASA GISS	x	x	
27	GISS-E2-H-CC	NASA GISS	x	x	
28	GISS-E2-R	NASA GISS	x	x	
29	GISS-E2-R-CC	NASA GISS	x	x	
30	HadCM3	MOHC	x	x	
31	HadGEM2-AO	NIMR/KMA	x	x	
32	HadGEM2-CC	MOHC	x	x	x
33	HadGEM2-ES	MOHC	x	x	x
34	INM-CM4	INM	x	x	
35	IPSL-CM5A-LR	IPSL	x	x	x
36	IPSL-CM5A-MR	IPSL	x	x	x
37	IPSL-CM5B-LR	IPSL	x	x	x
38	MIROC-ESM	MIROC	x	x	x
39	MIROC-ESM-CHEM	MIROC	x	x	x
40	MIROC4h	MIROC	x	x	
41	MIROC5	MIROC	x	x	x
42	MPI-ESM-LR	MPI-M	x	x	x
43	MPI-ESM-MR	MPI-M	x	x	x
44	MPI-ESM-P	MPI-M	x	x	x
45	MRI-CGCM3	MRI	x	x	x
46	MRI-ESM1	MRI	x	x	x
47	NorESM-M	NCC	x	x	x
48	NorESM-ME	NCC	x	x	

Note. Full expansions of CMIP5 model name and center acronyms are listed at https://www.ametsoc.org/PubsAcronymList.

Table 2.
CMIP6 models and variables used

Number	Model name	Model center	ua	psl	zg

1	ACCESS-CM2		x	x	x
2	ACCESS-ESM1-5		x	x	
3	AWI-CM-1-1-MR	AWI	x	x	
4	BCC-CSM2-MR	BCC	x	x	x
5	BCC-ESM1	BCC	x	x	x
6	CAMS-CSM1-0	CAMS	x	x	
7	CanESM5	CCCma	x	x	x
8	CESM2	NCAR	x	x	x
9	CESM2-FV2		x	x	x
10	CESM2-WACCM	NCAR	x	x	x
11	CESM2-WACCM-FV2		x	x	x
12	CNRM-CM6-1	CNRM-CERFACS	x	x	
13	CNRM-ESM2-1	CNRM-CERFACS	x	x	
14	E3SM-1-1	E3SM-Project	x	x	
15	FGOALS-f3-L		x	x	
16	FGOALS-g3		x	x	
17	FIO-ESM-2-0		x	x	
18	GFDL-CM4	NOAA-GFDL	x	x	
19	GISS-E2-1-G	NASA-GISS	x	x	x
20	GISS-E2-1-G-CC		x	x	
21	GISS-E2-1-H	NASA-GISS	x	x	
22	HadGEM3-GC31-LL	MOHC	x	x	x
23	HadGEM3-GC31-MM		x	x	
24	INM-CM4-8		x	x	
25	INM-CM5-0		x	x	
26	IPSL-CM6A-LR	IPSL	x	x	
27	MCM-UA-1-0		x	x	
28	MIROC6	MIROC	x	x	x
29	MPI-ESM-1-2-HAM		x	x	
30	MPI-ESM1-2-HR		x	x	x
31	MPI-ESM1-2-LR		x	x	x

32		MRI-ESM2-0	MRI	x	x	x
	33	NESM3		x	x	
	34	NorCPM1		x	x	
	35	NorESM2-LM	NCC	x	x	x
	36	NorESM2-MM		x	x	x
	37	SAM0-UNICON	SNU	x	x	
	38	TaiESM1		x	x	
	39	UKESM1-0-LL	MOHC	x	x	x

Note. Expansions of CMIP6 model center acronyms are listed at https://wcrp-cmip.github.io/CMIP6_CVs/docs/CMIP6_institution_id.html.

Table 3.
CMIP5 climatological annual mean westerly jet diagnostics

Model	JLI (degrees)	JLI bias (degrees)	JLI rank	JSI (m/s)	JSI bias (m/s)	JSI rank
ERA-Interim	-50.92		11	12.81		19
MMM	-49.01	1.91	27	13.12	0.31	25
*ACCESS1-0	-50.44	0.48	14	12.98	0.17	24
*ACCESS1-3	-50.50	0.42	13	13.88	1.07	36
*BNU-ESM	-47.57	3.35	36	15.19	2.38	49
CCSM4	-52.36	-1.44	4	14.93	2.12	46
CESM1-BGC	-52.27	-1.35	5	14.86	2.04	45
CESM1-CAM5	-52.01	-1.09	7	13.51	0.70	32
CESM1-FASTCHEM	-52.78	-1.86	3	14.85	2.04	44
CESM1-WACCM	-55.01	-4.09	1	14.56	1.75	43
*CMCC-CESM	-45.15	5.77	44	12.87	0.05	20
*CMCC-CM	-48.23	2.69	34	11.82	-1.00	7
*CMCC-CMS	-46.86	4.06	41	12.22	-0.59	9
*CNRM-CM5	-49.41	1.51	25	12.08	-0.73	8
CNRM-CM5-2	-50.33	0.59	16	12.24	-0.57	10
CSIRO-Mk3-6-0	-47.32	3.60	39	13.16	0.35	26
CanCM4	-48.86	2.06	29	13.70	0.89	34
*CanESM2	-48.99	1.93	28	13.76	0.95	35
*FGOALS-g2	-44.08	6.84	48	12.66	-0.15	15
FIO-ESM	-46.38	4.54	42	14.94	2.13	47
GFDL-CM2p1	-50.17	0.75	17	13.65	0.84	33
GFDL-CM3	-49.46	1.47	24	13.28	0.47	27
GFDL-ESM2G	-50.63	0.29	12	12.97	0.15	22

GFDL-ESM2M	-50.11	0.81	19	12.93	0.12	21
GISS-E2-H	-49.46	1.46	23	9.88	-2.93	1
GISS-E2-H-CC	-50.12	0.81	18	11.06	-1.75	4
GISS-E2-R	-48.43	2.49	33	11.20	-1.61	5
GISS-E2-R-CC	-48.63	2.29	31	11.23	-1.59	6
HadCM3	-49.32	1.60	26	13.92	1.10	37
HadGEM2-AO	-50.36	0.56	15	12.98	0.16	23
*HadGEM2-CC	-49.48	1.44	22	12.25	-0.57	11
*HadGEM2-ES	-49.66	1.27	21	12.72	-0.09	18
*IPSL-CM5A-LR	-43.68	7.24	49	12.59	-0.22	13
*IPSL-CM5A-MR	-44.89	6.03	46	12.54	-0.27	12
*IPSL-CM5B-LR	-44.85	6.07	47	10.33	-2.49	2
*MIROC-ESM	-45.15	5.77	45	14.33	1.52	40
*MIROC-ESM-CHEM	-45.43	5.49	43	14.38	1.57	41
MIROC4h	-48.54	2.39	32	14.48	1.67	42
*MIROC5	-46.95	3.97	40	10.57	-2.24	3
*MPI-ESM-LR	-47.51	3.41	37	12.69	-0.12	17
*MPI-ESM-MR	-47.65	3.27	35	12.64	-0.17	14
*MPI-ESM-P	-47.44	3.48	38	12.69	-0.13	16
*MRI-CGCM3	-51.52	-0.60	8	13.35	0.54	29
*MRI-ESM1	-51.40	-0.48	9	13.42	0.61	30
*NorESM1-M	-52.03	-1.11	6	13.46	0.64	31
NorESM1-ME	-52.80	-1.88	2	14.14	1.32	38
*bcc-csm1-1	-48.70	2.22	30	14.28	1.47	39
*bcc-csm1-1-m	-50.93	-0.01	10	15.15	2.33	48
inmcm4	-49.74	1.19	20	13.31	0.50	28

Note. The period used for defining climatologies is 1979-2005, which is the maximum-available overlap time across CMIP5, CMIP6 and ERA-Interim. The rankings for JLI are in order from most equatorward to most poleward, where individual models, the multi-model mean and reanalysis data are all included (i.e. a JLI ranking of 1 indicates the most equatorward jet). For JSI the ranking order is lowest to highest. Biases are relative to ERA-Interim. Asterisks indicate models used in the SAM decorrelation analysis shown in Figure 5.

Table 4.
As Table 3, but for CMIP6

Model	JLI	JLI bias	JLI	JSI (m/s)	JSI bias	JSI
ERA-Interim	-50.92		16	12.81		17
MMM	-50.49	0.43	20	13.32	0.51	22
*ACCESS-CM2	-49.99	0.93	26	12.72	-0.1	16
ACCESS-ESM1-5	-50.48	0.44	21	13.78	0.97	25
AWI-CM-1-1-MR	-51.04	-0.12	15	13.38	0.56	23
*BCC-CSM2-MR	-50.9	0.02	17	14.57	1.75	34
*BCC-ESM1	-50.47	0.45	22	14.94	2.13	38
CAMS-CSM1-0	-49.42	1.5	31	12.85	0.03	18
*CESM2	-51.87	-0.95	10	14.79	1.98	37
*CESM2-FV2	-52.9	-1.98	1	15.02	2.21	41
*CESM2-WACCM	-52.02	-1.1	9	14.97	2.15	40
CESM2-WACCM-FV2	-52.1	-1.18	7	14.71	1.9	35
CNRM-CM6-1	-48.12	2.81	39	12.38	-0.43	9
CNRM-ESM2-1	-48.77	2.15	36	12.47	-0.34	10
*CanESM5	-49.81	1.11	28	13.7	0.88	24
E3SM-1-1	-50.67	0.25	18	14.95	2.14	39
FGOALS-f3-L	-49.71	1.21	29	12.67	-0.14	15
FGOALS-g3	-49.53	1.39	30	14.72	1.9	36
FIO-ESM-2-0	-52.78	-1.86	2	13.79	0.98	26
GFDL-CM4	-49.08	1.84	35	13.11	0.29	20
*GISS-E2-1-G	-51.22	-0.3	12	12.56	-0.26	12
GISS-E2-1-G-CC	-51.2	-0.28	13	12.24	-0.57	6
GISS-E2-1-H	-51.41	-0.49	11	11.78	-1.03	3
*HadGEM3-GC31-LL	-50.32	0.6	23	12.49	-0.32	11
HadGEM3-GC31-MM	-49.25	1.67	33	11.74	-1.07	2
INM-CM4-8	-51.15	-0.23	14	12.34	-0.47	8

INM-CM5-0	-50.25	0.67	24	12.26	-0.55	7
IPSL-CM6A-LR	-49.12	1.81	34	12.21	-0.6	5
MCM-UA-1-0	-49.37	1.55	32	14.06	1.24	32
*MIROC6	-48.5	2.42	38	11.25	-1.56	1
MPI-ESM-1-2-HAM	-49.94	0.98	27	12.15	-0.66	4
*MPI-ESM1-2-HR	-48.75	2.17	37	12.62	-0.19	14
*MPI-ESM1-2-LR	-48.07	2.85	40	12.96	0.14	19
*MRI-ESM2-0	-47.83	3.09	41	13.2	0.39	21
NESM3	-50.64	0.28	19	13.83	1.02	28
NorCPM1	-52.72	-1.8	3	13.84	1.03	29
*NorESM2-LM	-52.61	-1.69	4	14.23	1.42	33
*NorESM2-MM	-52.58	-1.65	5	13.91	1.1	31
SAM0-UNICON	-52.09	-1.17	8	13.83	1.02	27
TaiESM1	-52.24	-1.32	6	13.84	1.03	30
*UKESM1-0-LL	-50.12	0.8	25	12.6	-0.21	13

Table 5.
CMIP5 models with the 12 most equatorward jet latitudes (upper quartile of JLI) and related CMIP6 models.

CMIP5 model	CMIP6 name close match*	CMIP6 models from the same model center
IPSL-CM5A-LR	IPSL-CM6A-LR	
FGOALS-g2	FGOALS-g3	
IPSL-CM5B-LR		IPSL-CM6A-LR
IPSL-CM5A-MR		IPSL-CM6A-LR
MIROC-ESM		MIROC6
CMCC-CESM		
MIROC-ESM-CHEM		MIROC6
FIO-ESM	FIO-ESM-2-0	
CMCC-CMS		
MIROC5	MIROC6	
CSIRO-Mk3-6-0		ACCESS-CM2, ACCESS-ESM1-5
MPI-ESM-P		MPI-ESM-1-2-HAM, MPI-ESM1-2-HR, MPI-ESM1-2-LR

Note. *Closely matching CMIP6 model names do not necessarily indicate closely related models.